49th AIAA Aerospace Sciences Meeting including the New Horizons Forum and Aerospace Exposition
4 - 7 January 2011, Orlando, Florida

AIAA 2011-957

# Induced Flow from Serpentine Plasma Actuators Acting in Quiescent Air

Ryan Durscher* and Subrata Roy†
*Computational Plasma Dynamics Laboratory and Test Facility, Applied Physics Research Group*
*Mechanical and Aerospace Engineering Department*
*University of Florida, Gainesville, FL 32611-6300*

**This paper presents experimental measurements performed on a dielectric barrier discharge (DBD) plasma actuator with the electrodes in a serpentine design. Such a configuration induces a local pinching or local spreading of the fluid as one follows along the span of the actuator. In this work the serpentine configuration is constructed from patterned circular arcs. The influence of applied voltage on the induced flow field is studied. To quantify these effects, stereo particle image velocimetry (PIV) is used to generate time averaged, spatially resolved measurements of the detailed flow structure. The three components of the velocity vector are measured along both spanwise and streamwise cuts. These slices are then reconstructed to provide a 3D view of the induced flow field. The results for the induced flow fields are also compared with 2D PIV measurements made on a standard linear DBD actuator.**

## Nomenclature

| | | |
|---|---|---|
| $I$ | = | instantaneous applied input current, A |
| $l_{span}$ | = | spanwise length of electrode, mm |
| $l_{eff}$ | = | effective length of electrode, mm |
| $p$ | = | serpentine period, mm |
| $P_{tot}$ | = | total power delivered to the actuator, W |
| $r$ | = | radius of serpentine curve, mm |
| $t$ | = | thickness of dielectric substrate, mm |
| $u_x$ | = | x-component of the induced flow velocity, m/s |
| $u_y$ | = | y-component of the induced flow velocity, m/s |
| $u_z$ | = | z-component of the induced flow velocity, m/s |
| $V$ | = | instantaneous applied input voltage, kV |
| $w$ | = | width of electrode, mm |
| $\omega_x$ | = | x-component of vorticity, 1/s |
| $\omega_z$ | = | z-component of vorticity, 1/s |

## I. Introduction

The dielectric barrier discharge (DBD) plasma actuator is a relatively simple device in design and operation. It is arguably due to this simplicity that it has received such considerable attention in recent years. For its operation, all one requires is a high voltage, alternating current (AC) source capable of peaks on the order of 5 to10 kV. The high voltage signal is then applied to a conducting electrode adhered to a dielectric substrate. A grounded electrode is placed asymmetrically on the lower surface of the dielectric with an additional dielectric layer covering it to avoid an unwanted discharge. The high potential difference between the two electrodes weakly ionizes the surrounding air. The presence of the plasma manifests itself as an induced body force on the fluid resulting in a tangential wall jet (figure 1). The induced flow, in quiescent air, is generally of a few meters per second.

* Graduate Student, Student Member AIAA, dursch@ufl.edu
† Associate Professor, Associate Fellow AIAA, roy@ufl.edu

Due to the DBD's relatively small influence on the surrounding medium, the range of Reynolds numbers in which these actuators have been used is relatively low.[1-3] In order to extend upon the operational usefulness of the actuators, numerous authors have investigated variations on the design and arrangement of the standard DBD plasma actuator. One such variation is the plasma synthetic jet actuator, or PSJA, investigated by Santhanakrishnan and Jacob[4]. The PSJA, as the name implies, creates a vertical jet away from the dielectric surface. The jet is produced by arranging the exposed electrode in a closed loop such that opposing discharges are generated. When the induced flows from the two discharges collide, they are directed upward. An array of linear plasma synthetic jets was used by Schatzman and Thomas[5] a streamwise vortex generator. The actuators were used to effectively mitigate separation resulting from turbulent flow over a convex ramp. Schatzman and Thomas[5] attributed the increase in control authority to the enhanced mixing as a result of the generated streamwise vortices.

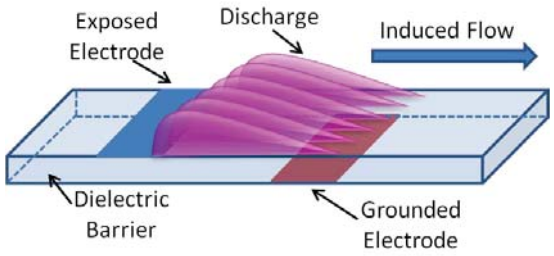


**Figure 1. Generic (standard) linear dielectric barrier discharge plasma actuator.**

As a modification to the above configurations, the serpentine design ensures a fully three-dimensional flow control mechanism that combines the effects of a standard linear actuator and a PSJA (figure 2). Intuitively, as one moves along the span of the actuator there is a spreading of the fluid at the crest while there is a pinching in the trough. One would then expect such as a disturbance to result in enhanced mixing of the surrounding fluid. This was numerically predicted by Roy and Wang[6] who applied the actuator to flow over a flat plate. The results of the simulation also show similar vortex generating capabilities to that of the actuator configuration used by Schatzman and Thomas in experiments described above. However, instead of using an array of actuators, only a single actuator is needed in the serpentine design. This could potentially lead to lower power consumption.

The experimental validation of the influence of a serpentine actuator on a freestream boundary layer is an area which still requires evaluation. However, in this paper we aim to explore and understand the operational mechanisms of the induced flow field generated by the serpentine configuration acting in quiescent air. The design is constructed from patterned circular arcs. The nonintrusive flow diagnostic technique of particle image velocimetry (PIV) is used to quantify the effects of the actuator. A stereo-PIV system is used to capture time averaged, spatially resolved data sets of the vector fields along spanwise and streamwise cuts. The 2D planes are then reconstructed to give a 3D view of the induced flow field for comparison with the prior numerical prediction of Roy and Wang[6].

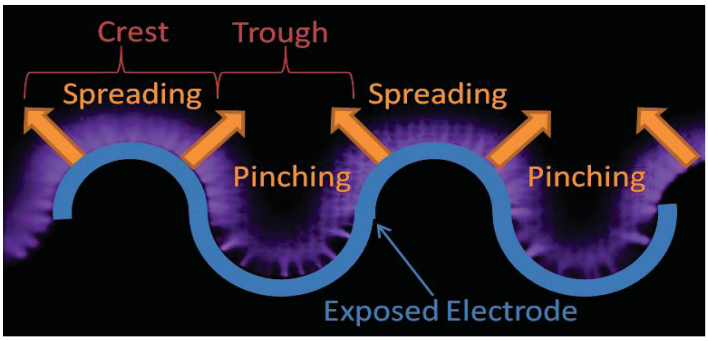


**Figure 2. Circular serpentine plasma actuator**

## II. Experimental Setup

### A. Serpentine Actuator Fabrication and Design

The most common technique, one could even say the state of the art, used in plasma actuator fabrication is simply cutting adhesively backed copper/aluminum tape with a razor blade and laying the strips of metal on a dielectric substrate by hand. This simplistic method for obvious reasons lacks dimensional control and introduces a great deal of error into the actuator design. A more troublesome aspect of this method, however, is that one is somewhat limited to rudimentary actuator configurations (i.e. straight lines). As a remedy we used a photo-

fabrication method to construct the continuous curved surfaces of the serpentine actuator. Such a method is widely used in the electronics community for in-house printed circuit board (PCB) fabrication.

Sheets of copper tape with a nominal thickness of 0.07 mm were first adhered to both sides of the acrylic dielectric substrate. The thickness, *t*, of the acrylic was 3.0 mm. A photosensitive negative dry film resist was then laid on top of the thin copper sheet. To help with adhesion of the resist to the copper/acrylic, hot air from a heat gun was blown on both sides of the actuator. The actuator design was printed on a transparent film with the desired features outlined by a dark background. The films have a minimum feature resolution of 25 μm, which is certainly below the millimeter dimensions of the designs. The transparencies were then aligned via alignment marks on both sides of the dielectric substrate and placed under a UV source for 15 minutes (each side) in order to expose the resist. A negative film developer was then gently brushed on to the actuator's surface to remove the unexposed resist. This results in a mask with the desired actuator design covering the copper tape. The actuator is then submerged in a ferric chloride bath to remove (via wet/chemical etching) the unwanted copper. The final step in the fabrication process is detaching the reminiscence of the adhesive glue left behind by the copper tape using a solvent such as methanol or acetone.

A general schematic of the serpentine design investigated in this work is shown in the following figure. The width of the exposed electrode, $w_1$, was fixed at 2 mm and there was no horizontal displacement between the electrodes. The patterned circular arcs of the inner edge of the exposed electrode in the design are 6 mm ($r_1$) and 4 mm ($r_2$) (figure 3b). The lower, grounded electrode has a width, $w_2$, of 5 mm which follows along the inner radius of the exposed electrode. Based on the provided dimensions one can calculate the total period, *p*, of design as 20 mm. To prevent end effects from influencing the velocity measurements, the tested actuators consisted of 8 periods. This corresponds to overall spanwise (z-direction) lengths, $l_{span}$, of 160 mm.

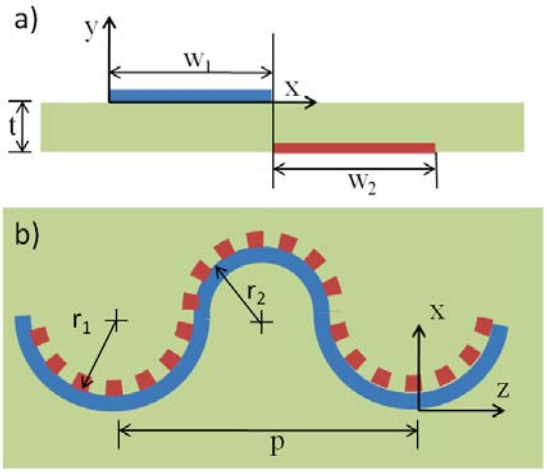


**Figure 3. Schematics of the serpentine actuator tested with a) corresponding to a side profile, while b) is a top view. (Not to scale)**

### B. Plasma Generation and Power Measurements

The high voltages required to ignite the plasma discharge were generated using a Corona Magnetics Inc. high voltage transformer. A 10 kHz, sinusoidal waveform was first produced using a Tektronix arbitrary waveform generator (AFG3022B) and was further amplified using a QSC audio amplifier (RMX 2450). A circuit schematic is provided in figure 4. The voltage and current delivered to the actuator were monitored using a Tektronix high-voltage probe (P6015A) along with a Pearson Electronics ammeter (2100). The output from the probes was sampled at 250MSa/s using a digitizing oscilloscope (Tektronix DPO3014). In a single acquisition the oscilloscope was set to capture 1.0E6 points. As such, 10 acquisitions were seized for each input voltage which corresponds to 560 periods over which the power delivered to the actuator is averaged. The total mean power, $P_{tot}$, was calculated simply by summing the product of the instantaneous voltage, *V*, and current, *I*, waveforms and dividing by the total number of points.

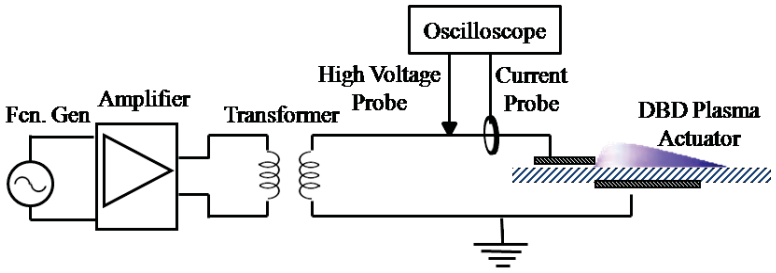


**Figure 4. Plasma generation circuit used to power the serpentine plasma actuators.**

### C. Particle Image Velocimetry

The standard linear plasma actuator is generally considered to be a two dimensional device, indicating that the body force vector only has two components (x, y). This assumption does not hold however for the serpentine design. By nature of the configuration, fluid will be pushed in all three directions. To capture these effects, we use a stereoscopic particle image velocimetry system to spatially resolve the three components of induced velocity vectors for a given 2D plane.

The actuator is setup in a 61 cm x 61 cm x 120 cm quiescent chamber shown in figure 5. The floor of the chamber is connected to a single axis manual traverse (Velmex A1503P40-S1.5), which allows the floor to translate horizontally ±19 mm off center. This provides the ability to easily make measurements along specific spanwise or streamwise locations in order to fully map out the three dimensional effects of these actuators without having to reposition the light sheet or adjust the cameras optics.

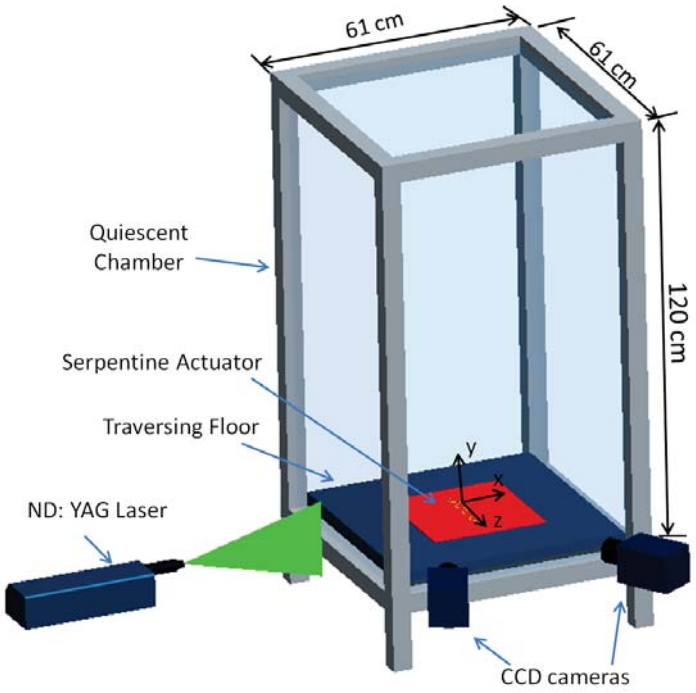


**Figure 5. Stereo PIV setup**

For each spanwise and streamwise cut, 200 image pairs were taken. Two of *LaVision*'s ImagerPro X 4M (2048 x 2048 pixels) cameras in combination with 105 mm macro lenses and 1.4x teleconverters were used to capture the PIV images. The field of view for each image was approximately 45 mm x 45 mm. A light sheet cutting along the span of the actuator was generated using a Nd:YAG, dual cavity pulsed, 532 nm laser (New Wave Research Solo PIV II 30). The sheet illuminated vaporized Ondina oil which was used to seed the chamber. The oil particles were generated by TSI atomizer (Model 9302). The atomizer produces a droplet with a mean diameter of ~0.8 μm when pressurized at 25 psi.[7] The surface of the dielectric was coated with rhodamine paint to minimize the glare resulting from the light sheet striking the bare acrylic. Also, note that care was taken not to spread the paint on the electrode or in an expected discharge region. Ideally a narrow band-pass filter (532nm) would have been attached to the end of each lens to further block the shifted light due to interaction with the rhodamine. However, a mismatch in image intensity between the camera in forward scatter and the camera in back scatter plagued the setup regardless of aperture settings when the filters were applied. *LaVision*'s DaVis 3D PIV software package was used to calibrate, capture, pre-process, and post-process the PIV images.

## III. Results

In order to fully capture the three dimensional nature of the induced flow field, both spanwise and streamwise cuts were taken along 2D planes of the actuator. For the spanwise cuts, 9 planes were imaged starting at z = 0 mm and ending at z = -20 mm in -2.5 mm increments. Note that the total period of the device is 20 mm; therefore a complete period was captured in the spanwise scan. Similarly, 10 planes were captured in the streamwise direction starting at x = -2.5 mm and ending at x = 20 mm, again in 2.5 mm increments. Figure 6 provides an example of spanwise and streamwise planar cuts represented by orange (dashed) and purple (dotted) lines, respectively. The following section presents the results of these measurements and highlights how the serpentine design differs from that of a standard linear actuator (figure 1).

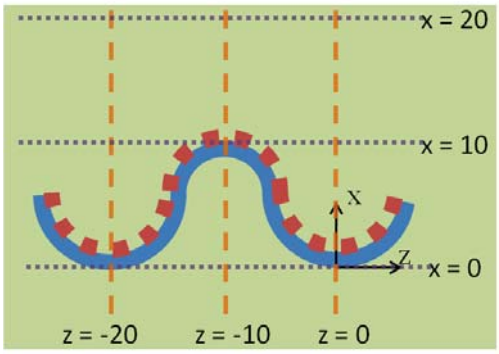


**Figure 6. Example of spanwise (orange dashed lines) and streamwise (purple dotted lines) planar cuts. (Not to scale)**

### A. Flow Visualization

As a simple first step in qualitatively determining the influence of a circular serpentine actuator operating in quiescent air, the laser sheet was positioned as to illuminate the spanwise plane cutting through the trough of actuator (z = 0 mm). A lit incense stick was placed near the exposed electrode, the actuator was turned on, and the image was captured using a Nikon D90 SLR camera. The result of this rudimentary test indicated that there was a pinching of the fluid along the plane due to the curved geometry of the electrode. This resulted in the fluid being pushed away from the surface at approximately a 43° angle (figure 7a). As a comparison smoke flow visualization was done with a standard linear actuator (figure 7b), in which the convecting flow was found to create a ~12° angle with the surface. The observed biased pinching of the fluid could only result if the plasma body force is acting perpendicular to exposed electrode. If this is the case, the serpentine actuator would truly introduce a complicated 3D nature to the induced flow field, since a vector perpendicular to the exposed electrode is pointing out of the (typical) x-y plane over most of the span.

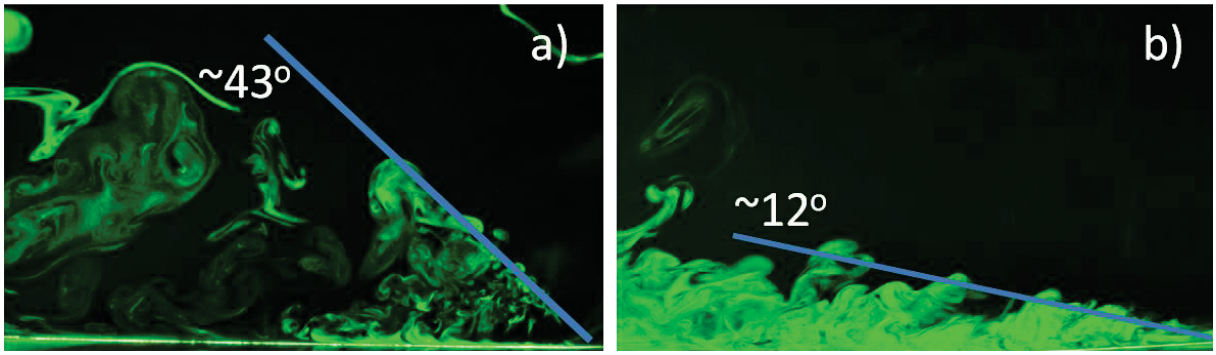


**Figure 7. Instantaneous smoke flow visualization: a) Circular patterned serpentine actuator (plane taken along the trough) and b) standard linear actuator.**

### B. PIV Results for the Serpentine Actuator

If the serpentine actuator is truly a three dimensional device, as one moves along the span of the actuator, the z-component of velocity, $u_z$, and resulting flow structure should vary. This fact is shown in figure 8 which depicts contours of $u_z$ for select spanwise locations for an input voltage of 14kVpp. One can see that at the troughs (z = 0 mm and z = -20 mm) and the crest (z = -10 mm) of the actuator the flow direction is primarily in the x-y plane (or 2D). It is pertinent to note, however, that for z = -20 mm there is some out of plane (z) velocity. A possible explanation for this is a non-uniform plasma formation due to imperfections in the actuators construction. Such flaws could lead to local concentration points in the electric field resulting in variations in the plasma force on either side of the plane. For the other locations (z = -2.5 mm and z = -17.5 mm) presented in figure 8, one can see that the actuator is adding an out of plane component to the net momentum imparted to the fluid. It will be shown later that

this out of plane component results in streamwise counter rotating vortex pairs. The paired velocity contours in and out of plane shown in figure 8b and 8d are further evidence of the vortex pairs.

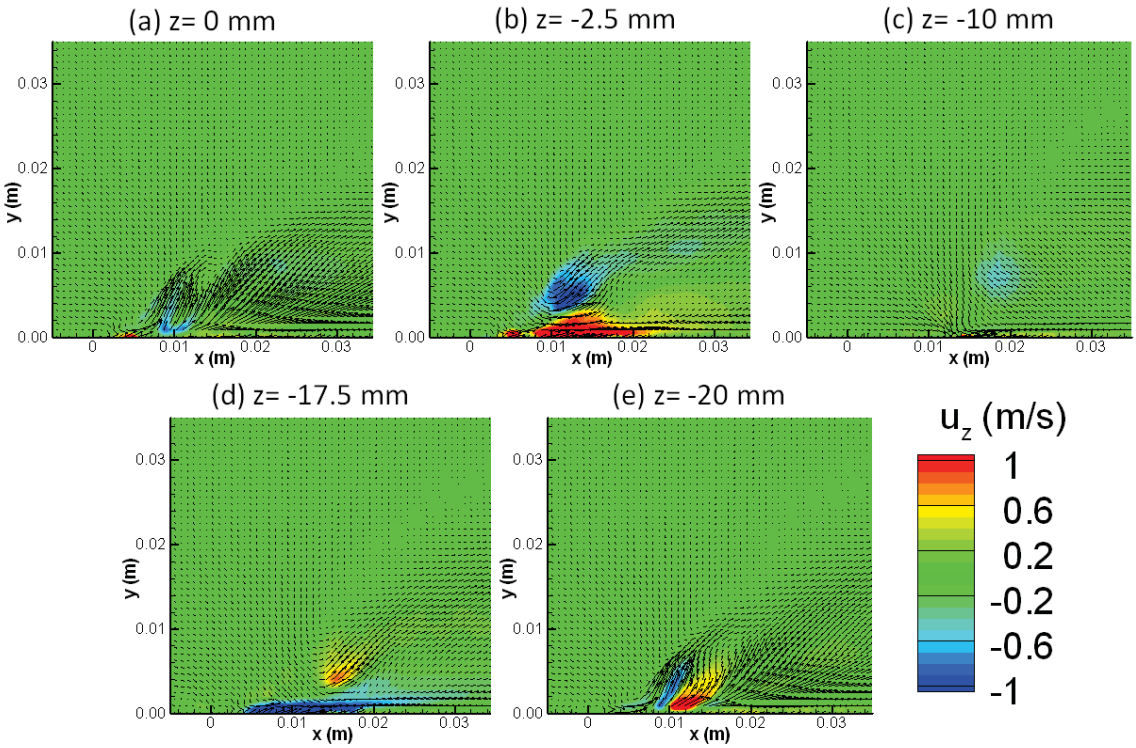


**Figure 8. Time averaged z-velocity (m/s) contours overlaid with x and y-velocity vectors for various planar cuts along the span of a circular serpentine actuator (14kVpp). a) z = 0 mm, b) z = -2.5 mm, c) z = -10 mm, d) z = -17.5 mm, and e) z = -20 mm.**

Although this work is primarily concerned with time averaged data it is interesting and intuitive to look at an instantaneous snapshot of the induced flow field. Presented in figure 9 is a contour plot of the z-velocity taken along z = 0 mm (trough) at a random instant in time. One can see that at this particular instant there is a staggered structure to the out of plane velocity component. This is interesting since the time averaged data indicates that the flow is primarily 2D along this plane. Therefore, in order for there to be a zero mean, there must be a constant fluctuation in the velocity vector such that there is net cancelation. Similar plots may be shown for z = -10 mm as well. These results suggest that there are small scale temporal effects contributing to the flow actuation in serpentine design which need to be explored. Future efforts will address the temporal nature of this actuator configuration through phase locked stereo-PIV measurements.

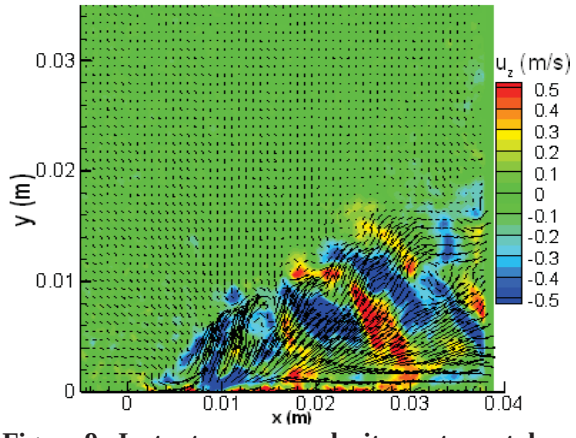


**Figure 9. Instantaneous z-velocity contours taken at z = 0 mm**

Reassembled 3D perspectives and planar contours of the time averaged z-vorticity for the circular serpentine actuator are shown in figure 10. Based on vorticity alone, the plots are reminiscent of a typical wall jet produced by a linear actuator over the majority of the span. The primary deviations arise at or near the troughs of the actuator. From the iso-surfaces plot (figure 10a) one can see that there is a protrusion in $\omega_z$ away from the surface at these locations due to the opposing plasma forces pushing the fluid upward. This is more clearly shown in figure 10c.

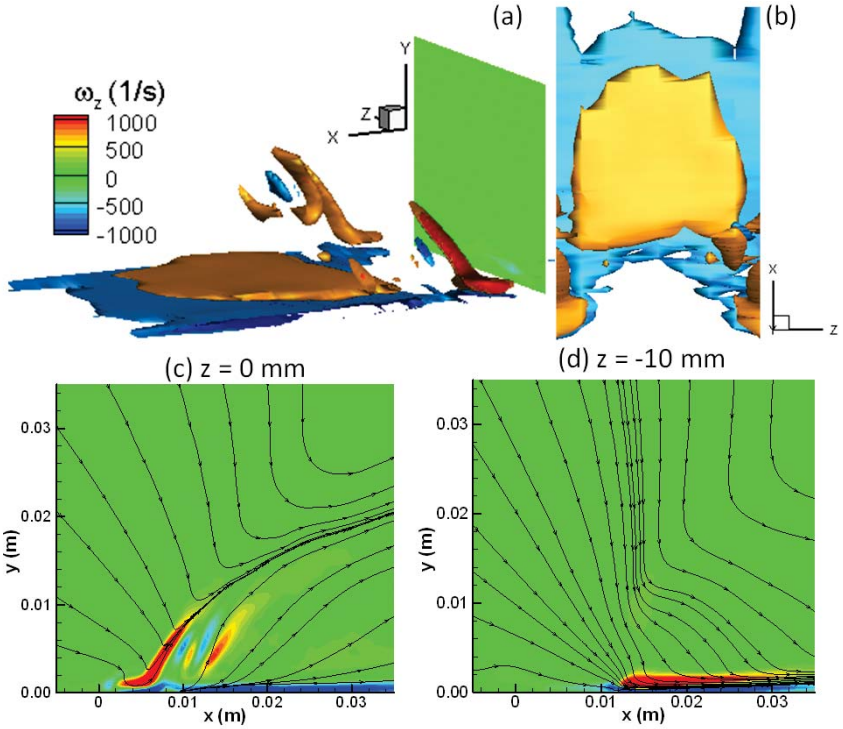


**Figure 10. Mean spanwise (z) vorticity ($s^{-1}$) iso-surfaces reconstructed from planar measurements on a circular serpentine actuator with a driving potential of 14kVpp: a) perspective and b) top views (the green plane indicates x=0mm). Planar contours and streamtraces extracted at z = 0 mm (c) and z= -10 mm (d).**

Select results from the streamwise scan of the circular serpentine actuator are shown in figure 11, which depicts contours of the streamwise ($\omega_x$) vorticity. In examining the figure one finds pairs of the counter rotating vortices which are centered along the z = 0 mm and z = -20 mm planes (the troughs of the actuator). The vortices begin to form around the inflection point (x = 6 mm) of the curve making up the exposed electrode and continue to grow in magnitude as they propagate downstream. The growth of the vortex pairs is clearly seen in figure 11d. These results agree well with prior work done by Roy and Wang[6], who numerically predicted the existence of such a flow structure. However, one may also notice the lack of symmetry between the vortex pair located at z = 0 mm and the one at z = -20 mm. The asymmetry appears to worsen the further downstream one looks. Such a result is most likely due to slight variations in the plasma body force (due to minor imperfections in the actuator construction) which results in a natural non-uniformity in the flow field.

As previously mentioned the streamwise vorticity is a direct result of the out of plane (z) forcing that the serpentine design imparts to the fluid. This out of plane component does not exist with a conventional linear actuator. It was also shown above that at specific locations, the serpentine configuration acts similar to that of a linear actuator. Therefore, the serpentine design is not only capable of inducing streamwise vorticity, but spanwise as well. Such a device has numerous aerodynamic applications where increased mixing of the local fluid is required or desired. The areas of boundary layer transition, convective heat transfer, and plasma assisted combustion (PAC) immediately come to mind. In all of these situations, an improvement in flow turbulization can significantly enhance the desired output.

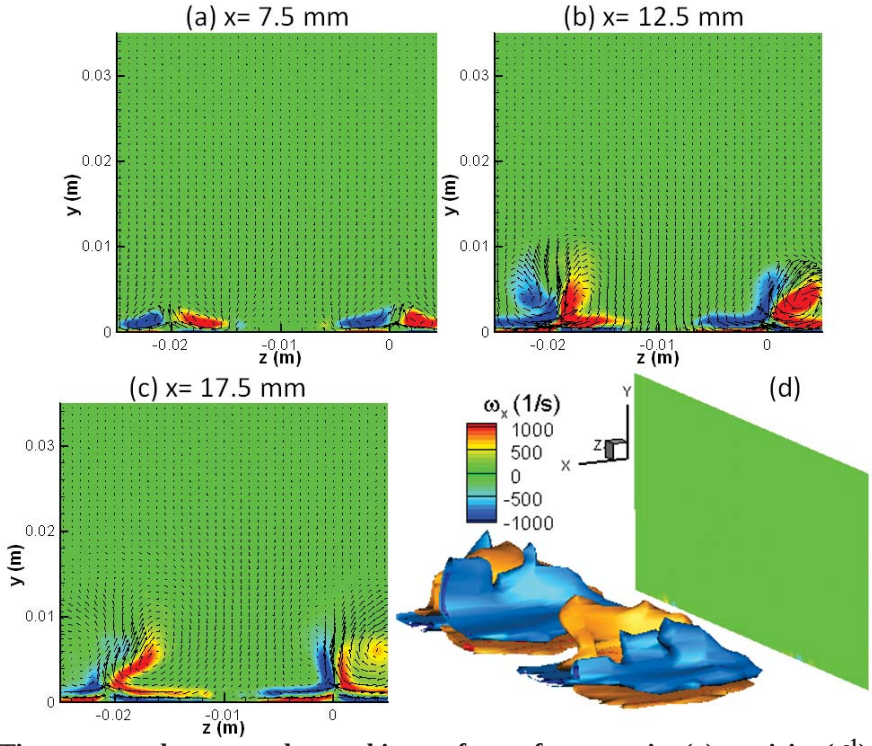


**Figure 11. Time averaged contour plots and iso-surfaces of streamwise (x) vorticity ($s^{-1}$) for a circular serpentine actuator with an input voltage of 14kVpp: a) x = 7.4 mm, b) x = 12.5 mm, c) x = 17.5 mm and d) a 3D perspective view (the green plane indicates x=0mm).**

### C. Effects of Voltage for a Serpentine Actuator

To investigate the influence that input voltage has on the structure of the induced flow, the supplied voltage was increased from 14kVpp to 16kVpp. For this comparison, only spanwise cuts were taken. Figure 12 presents reassembled 3D perspectives and planar contours of the time averaged z-vorticity for the higher driving potential. In comparing the overall flow structure found in figures 12a and 12b with that of 10a and 10b the results are quite similar. Again with an input voltage of 16kVpp the z-vorticity shows characteristics of a typical wall jet from a linear actuator over much of the span of the actuator, with the exception being at the troughs (z = 0 mm and z = -20 mm). As before, at these locations the opposing plasma forces result in a pinching of the fluid which is then propelled upward. Further comparing figures 12c and 12d with 10c and 10d one can see that the region over which the same magnitude of vorticity acts has increased with increasing voltage (particularly close to the wall). This increase is not surprising given that vorticity is directly tied to velocity, which is then proportional to voltage for a DBD actuator. An increase in velocity is indeed occurring as shown in figure 13. The absolute value of the peak velocity over the entire measured span increases from ~2.9 to ~3.4 m/s for the raise in voltage. Despite this increase, the velocity profiles (and underlying force mechanism) do not appear to change as figure 13 reveals for locations z = 0 mm and z = -10 mm. At the trough specifically, the resultant flow angle denoted in figure 13 by a solid black line, remains constant at ~38°. Note that this angle matches well with the angle estimated from flow visualizations described above. It is logical to speculate that the flow angle should vary as the voltage is increased since the resultant force on the fluid is increased as well. One would think that a larger force in the out of plane component would result in a stronger pinching effect, only to increase the impingement angle. However, based on the current data we conclude that beyond some threshold voltage the induced flow angle does not change. This result may be due to the fact that even though the plasma force is increasing, the forcing angle remains constant since the electrode geometry is fixed.

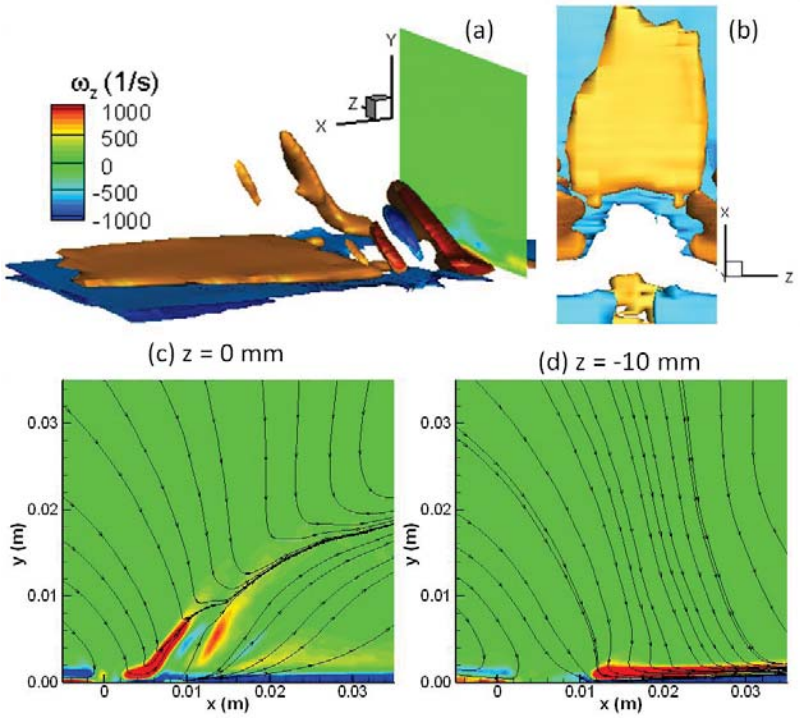


**Figure 12. Averaged spanwise (z) vorticity ($s^{-1}$) iso-surfaces reconstructed from planar measurements on a circular serpentine actuator with a driving potential of 16kVpp: a) perspective and b) top views (the green plane indicates x=0mm). Planar contours and stream traces extracted at z = 0 mm (c) and z= -10 mm (d).**

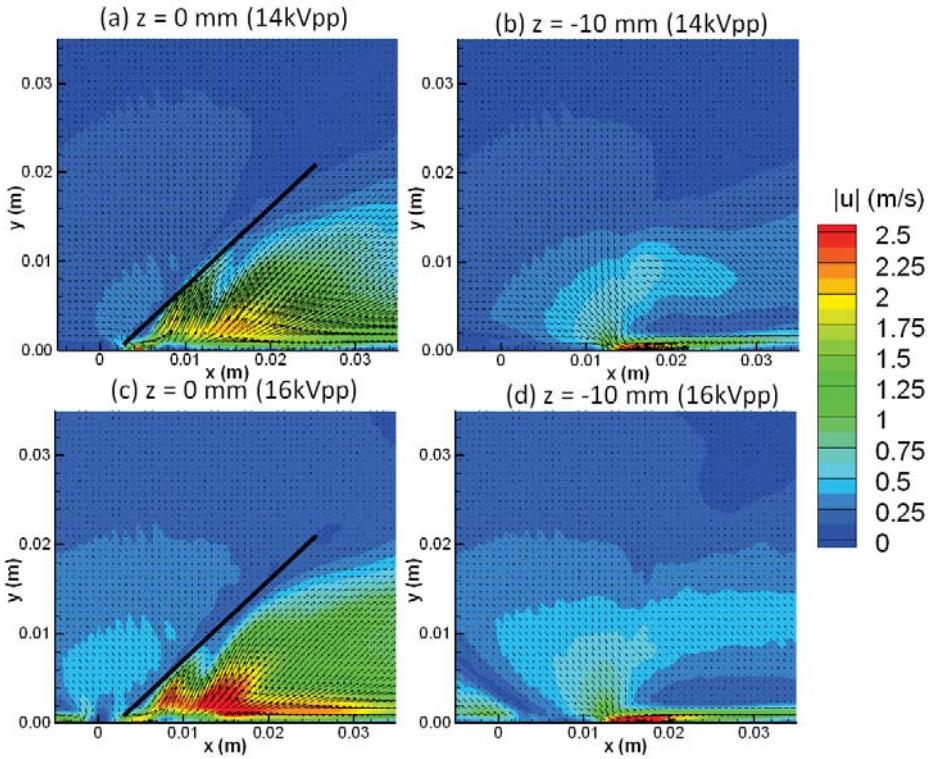


**Figure 13. Time averaged velocity magnitude contours at the z = 0 mm and z = -10 mm planes along a circular serpentine actuator for input voltages of 14kVpp (a and b) and 16kVpp (c and d). The impingement angle in the flow, which was found to be ~38°, is indicated by the black solid line.**

### D. Comparison with a Linear Actuator

2D PIV planar measurements were made along the span of standard linear DBD actuator acting in quiescent air as a means of comparison. Testing conditions and experimental setup were identical to what has been described earlier with two exceptions. One, only a single camera was used (hence 2D PIV), and two, the electrode widths and length deviated slightly. Referring to figure 3a, $w_1$ = 5 mm and $w_2$ = 15 mm for the electrode widths, while the overall length, $l$, of the actuator was 160 mm. X and y-velocity profiles for two different spanwise locations (x = 15 mm and x = 20 mm) are presented in figure 16. The spanwise cut for the serpentine cases was taken along the trough (z = 0 mm), which was shown above to be quasi two dimensional. The resulting profiles presented in figure 16 highlight key differences in the actuator designs (linear and serpentine). In the case of the linear DBD the momentum injection is primarily in the x-direction which is localized near the wall. As a result there is little to no vertical (y) component of velocity. The serpentine configuration on the other hand introduces both x, y, and z (referring to figures 8 and 16) momentum to the fluid.

The average calculated power consumption is presented in table 1. When normalized by the spanwise length, $l_{span}$, the linear actuator clearly used less power than the serpentine design. However, as the name implies, the spanwise length only takes into account the spanwise extension of the device and does not consider the out of plane protrusion due to the patterned nature of the serpentine design. Defining a new length scale, $l_{eff}$, to account for the serpentine's winding electrode the normalized power is decreased. The power variations between the different actuator designs are now zero. Such a result is not surprising since the electrode geometry is being altered, not the ionization process. However, from a design perspective, the ultimate goal is to apply these actuators to real world aerodynamic flows such as over an airfoil. In such a case the actuator would most likely be applied over some unit length of the airfoil, where $P_{tot}/l_{span}$ would be the more appropriate design parameter.

**Table 1. Total power consumption for the tested actuators**

| | $P_{tot}$ (W) | $P_{tot}/l_{span}$ (W/m) | $P_{tot}/l_{eff}$ (W/m) |
|---|---|---|---|
| **Linear** | 3.2 | 20 | 20 |
| **Circular Serpentine** | 4.8 | 30 | 20 |

## IV. Conclusions

Stereo particle image velocimetry has been used to capture the complicated three dimensional flow field induced by serpentine plasma actuators in a quiescent environment. The design investigated in this study was constructed from patterned circular arcs. The actuator was found to inject x, y, and z momentum resulting in coherent three dimensional vortical structures. In particular, counter rotating vortex pairs in the streamwise direction were generated periodically along the span of the actuator. The serpentine actuator was further compared with a standard linear actuator. Future efforts will explore other design configurations such as patterned rectangles.

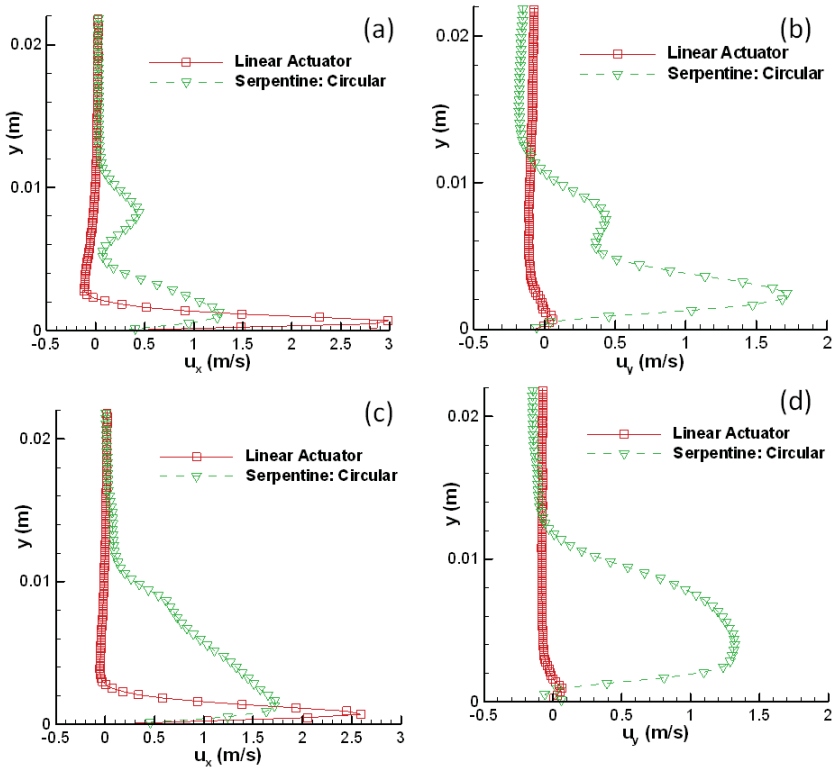


**Figure 14. $u_x$ and $u_y$ profiles taken at x = 15 mm (a and b) and x = 20 mm (c and d) spanwise locations for a linear and circular serpentine actuator. The input voltage for the actuators was 14kVpp**

## Acknowledgements

This work was partially supported by AFOSR grant #FA9550-09-1-0372 monitored by Dr. Douglas Smith.

## References

[1]Benard, N., Braud P., Jolibois, J., Moreau, E.,"Airflow Reattachment Along a NACA 0015 Airfoil by Surfaces Dielectric Barrier Discharge Actuator – Time Resolved Particle Image Velocimetry Investigation," *4th Flow Control Conference*, AIAA 2008-4202 Seattle, WA, June 2008.

[2]Huang, J., Corke, T. C., and Thomas, F. O., "Plasma Actuators for Separation Control of Low-Pressure Turbine Blades," *AIAA Journal*, Vol. 44, No. 1, 2006, pp 51- 57.

[3]Sung, Y., Kim, W., Mungal, M. G., and Cappeli, M., "Aerodynamic Modification of Flow over Bluff Objects by Plasma Actuation," Experiments in Fluids, Vol. 41, No. 3, Sept. 2006, pp. 479–486.

[4]Santhanakrishnan A. and Jacob, J., "Flow control with plasma synthetic jet actuators," *J. Phys. D: Applied Physics*., Vol. 40, 2007

[5]Schatzman, D. M. and Thomas, F. O., "Turbulent Boundary Layer Separation Control with Plasma Actuators," *4th Flow Control Conference*, AIAA Paper 2008-4199, Seattle, WA, June, 2008.

[6]Roy, S. and Wang, C., "Bulk flow modification with horseshoe and serpentine plasma actuators," *J. Phys. D: Applied Physics*., Vol. 42, 2009

[7]Model 9302 Atomizer, Instruction Manual, TSI, September, 2000